Validation of Antenna Modeling Methodology in IMT-Advanced Channel Model

Chun Pan*, Jianhua Zhang* and Feng Pei*
*Key Laboratory of Universal Wireless Communications, Ministry of Education
Wireless Technology Innovation Institute
Beijing University of Posts and Telecommunications, China
Email: panchun1987@gmail.com

***Abstract*—In this paper, the antenna modeling method in the International Mobile Telecommunications-Advanced (IMT-Advanced) channel model is validated by field channel measurements in the indoor scenario at 2.35 GHz. First, the 2×2 MIMO channel impulse responses (CIRs) are recorded with practical antennas as references. Second, the CIRs are reconstructed from the available IMT-Advanced channel model with field patterns of the practical antennas and updated spatial parameters extracted from the similar scenario measurements. Then comparisons between the field CIRs and the reconstructed CIRs are made from coherent bandwidth, eigenvalue dispersion, outage capacity, and ergodic channel capacity. It is found that the reconstructed results closely approximate real results in the coherent bandwidth and correctly describe the statistical characteristics in frequency domain. Compared to the field CIRs, the spatial correlation of the reconstructed CIRs with either type of antenna have a wider range, that causes the underestimation of the 5% channel outage capacity. Due to the negligence of the coupling among the antennas and the near field effect of antenna, this modeling method will have a great impact on the characteristic of radio channel, especially on the spatial characteristics.**

***Index Terms*—Multiple-input-multiple-output (MIMO), channel measurements, channel modeling, channel capacity.**

I. Introduction

Multiple-input multiple-output (MIMO) systems have been considered as one of the most promising approaches for high data rate without extra bandwidth. It was shown that the potential channel capacity of such systems grows linearly with antenna pairs in the independent identically distributed (i.i.d.) channel model [1], [2], but the channel fading correlation affects the capacity by modifying the distributions of the gains of these parallel channels [3]. According to this, the capacity ultimately depends on the channel model used.

Recently, to obtain an accurate channel capacity estimation, many verified channel models [4] were used. In [5], a model based on the Kronecker structure has been assumed to analyze the channel capacity and extended to a wideband MIMO channel model in [6]. But in [7], it was confirmed that the Kronecker model can not describe the multipath structure correctly. For example, the 8×8 MIMO capacity predicted by the Kronecker model is always below the capacity calculated directly from the filed measurement. Another important wideband MIMO spatial channel model, the International Mobile Telecommunications-Advanced (IMT-Advanced) channel model, is regarded as an appropriate channel model to predict the MIMO channel capacity. This channel model is based on the concept of the double-directional mobile radio channel [8]. By separating multipath radio channel model (including antenna) into multipath propagation channel model (including none of the antennas) and antenna pattern model independently, the model not only characterizes the multipath channel parameter but also can be configured with any type of antenna array. So this model is popular to investigate the impact of antenna array configuration on the capacity. The effects of the user's presence on the performance of MIMO system in data and in voice usage scenarios are investigated in [9].

To the author′s knowledge, there are few investigations to validate this modeling methodology in the IMT-Advanced channel model. Although this modeling method is convenient to analyze the influences of different antenna configurations on the channel characteristics, during channel modeling this model ignores some nonideal antenna issues which will influence the propagation characteristics, such as the correlation between antenna and propagation channel at near field of antennas, coupling among the antennas. So it is not clear if it is accurate enough to model the channel response by combining the antenna pattern and multipath propagation channel uncorrelatedly.

In this paper, the field measured MIMO channel impulse responses (CIRs) are firstly recorded with practical dipole antenna (DPA) and real terminal planar inverted-F antenna (PIFA) [10] as references. Second, the CIRs are reconstructed from the IMT-Advanced channel model with updated spatial parameters which measured with Omni-Directional Antenna array (ODA) and extracted by Space Alternating Generalized Expectation maximization (SAGE) algorithm. The practical antenna array response is also incorporated. Then comparisons between the field data and the reconstructed data are made from some metrics of MIMO channel [11], such as coherent bandwidth, eigenvalue dispersion, and channel capacity.

The remainder of the paper is organized as follows. The statistical channel model, channel measurements, and data post-processing are introduced in Section 2. Section 3 presents the results and the analysis. The analysis of channel characteristics are presented, e.g. the frequency domain in Sections 3.1 and the spatial domain in Sections 3.2, respectively. The capacity analysis are presented in Section 3.3. Conclusions are drawn in Section 4.

II. Validation Framework

A. Channel Model - IMT-Advanced

In the IMT-Advanced channel model [12], the spatial and temporal distributions are parameterized to characterize the MIMO channel. The parameters of all subpaths are calculated for each channel realization. A MIMO channel response $\mathbf{H}(t_0, \tau_n)$ at t_0 is created by IMT-Advanced program for each path through the superposition of the subpaths. The linear time variant response is defined by a matrix of dimension $U \times S$, where U is the number of receiving antennas and S is the number of transmitting antennas. The entries $h_{u,s}(t_0, \tau_n)$ of $\mathbf{H}(t_0, \tau_n)$ are

$$\begin{aligned} h_{u,s}(t_0, \tau_n) = \sum_{m=1}^{M} & \mathbf{F}_{rx,u}^{T}(\Omega_{n,m}) \mathbf{A}_{n,m} \mathbf{F}_{tx,s}(\Phi_{n,m}) \\ & \times \exp(j d_u 2\pi \lambda_0^{-1} \sin(\Omega_{n,m})) \\ & \times \exp(j d_s 2\pi \lambda_0^{-1} \sin(\Phi_{n,m})) \\ & \times \exp(j 2\pi f_{d,n,m} t_0). \end{aligned} \quad (1)$$

The index u and s correspond to the receiving and the transmitting antenna elements, respectively. The λ_0 is the wavelength of the carrier.The number of paths is indexed by n and the number of the subpaths are m. The $\mathbf{F}_{rx,u}$ and $\mathbf{F}_{tx,s}$ are defined as the field pattern of the receiving and the transmitting antenna elements. The d_u stands for the distance between the u^{th} receiving antenna element and the first element. For transmitting antenna elements, the d_s holds the same meaning with the d_u. The τ_n, $f_{d,n,m}$, $\Phi_{n,m}$ and $\Omega_{n,m}$ denote the propagation delay, the doppler shift, the azimuth of departure (AoD), and the azimuth of arrival (AoA) of the (n, m) propagation subpath. And the polarization matrix of the (n, m) subpath is defined by $\mathbf{A}_{n,m}$.

B. Validation methodology

In order to focus on the feasibility of this methodology, the CIRs $\mathbf{H}(t, \tau)$ are obtained respectively by the field measurement and the model reconstruction. The direct data (filed measured) $\mathbf{H}^{meas}$ are recorded by channel sounder with DPA array and the real terminal PIFA. The indirect data $\mathbf{H}^{model}$ are reconstructed by IMT-Advanced channel model with antenna pattern of the antenna array used in direct data recording and propagation channel parameters set extracted from the measurement with ODA in the same scenario.

Lots of channel measurement campaigns are conducted to obtain the raw data. According to the specific requirement, three types of measurement antenna arrays are needed, including DPAs, PIFA, and ODA. Furthermore, the antenna patterns of DPA and PIFA need to be calibrated as $\mathbf{F}^{DPA}$ and $\mathbf{F}^{PIFA}$ before measurement. The collected data with ODA are classified as $\mathbf{H}_{ODA}$, this measured data are used to extract the channel parameters. Then $\mathbf{H}^{model}$ are obtained by channel reconstruction with these channel parameters and the corresponding antenna pattern. At the end of data acquisition, four groups of CIRs are obtained. They are $\mathbf{H}_{DPA}^{meas}$ collected from field measurement with DPAs, $\mathbf{H}_{PIFA}^{meas}$ collected from field measurement with PIFA, $\mathbf{H}_{DPA}^{model}$ reconstructed by IMT-Advanced channel model with the antenna pattern of DPAs, and $\mathbf{H}_{PIFA}^{model}$ reconstructed with the antenna pattern of PIFA. Finally, the analysis on the channel characteristics will be performed.

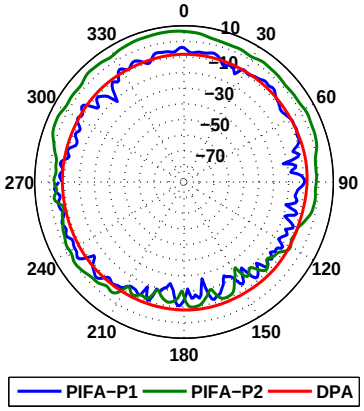

Fig. 1. Measured radiation patterns (in dBi) on the azimuth plane (x-y)

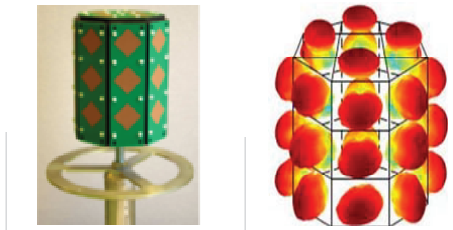

(a) (b)

Fig. 2. The configurations and antenna pattern of ODA: (a) antenna structure; (b) antenna pattern

C. Measurement Antenna

The field CIRs $\mathbf{H}^{meas}$ are collected by using DPA and PIFA as measurement antenna array. At transmitter (Tx), two DPAs with $4\lambda_0$ antenna spacing are used. Meanwhile two DPAs with $1/2\lambda_0$ antenna spacing and a basic PIFA are used at receiver (Rx) respectively. The patterns measured in dBi on the azimuth plane $(x - y)$ for all antennas are given in Figure 1. Both $\mathbf{F}^{DPA}$ and $\mathbf{F}^{PIFA}$ are the field radiation patterns of DPA and PIFA near the laptop.

In order to capture the multipath channel parameters in high accuracy, the ODA consisting of 56 cross-polarized elements is used at Tx and Rx. Figures 2 (a) and 2 (b) depict respectively the structure and antenna pattern of ODA.

D. Measurement System and Environment

An extensive measurement campaign is performed at center frequency of 2.35 GHz with 50 MHz bandwidth, using the Elektrobit PropSound channel sounder. As described in detail

in [13], the sounder works in a time-division multiplexing (TDM) mode. Thus periodic pseudo random binary signals are transmitted between different Tx - Rx antenna pairs in sequence. The interval within which all antenna pairs are sounded once is defined as a measurement cycle. Some important characteristics of measurement setup can be found in Table I. Because of the bandwidth limit of data bus and the number of antenna element, the code length of measurement system is configured as 63 when using ODAs as test antennas.

TABLE I
MEASUREMENT PARAMETERS SETTING.

Parameters	Setting
Carrier Frequency	2.35GHz
Bandwidth	50MHz
Code Length	255(DPA,PIFA), 63(ODA)
Tx Antenna Number	2(DPA), 32(ODA)
Rx Antenna Number	2(DPA or PIFA), 56(ODA)

E. Data Post Processing

In data post processing, the CIRs are converted from the raw data firstly. Due to the influence of the band-pass filter in measurement system, 10% high frequency component of baseband signal is cut during the post processing. The field CIRs $\mathbf{H}_{DPA}^{meas}$ and $\mathbf{H}_{PIFA}^{meas}$ are used as the direct CIRs $\mathbf{H}^{meas}$. And SAGE algorithm is applied to extract channel parameters from the CIRs $\mathbf{H}_{ODA}$. As an extension of Maximum-Likelihood (ML) method, the SAGE algorithm provides a joint estimation of the parameter set $\theta_l = \{\tau_l, f_{d,f}, \Phi_l, \Omega_l, \alpha_l\}$, $l = \{1, \cdots, L\}$, with no constrains on the response of antenna array. The definition of all these parameters are same as subsection A. In order to capture all dominant paths that characterizes the propagation environment exactly, totally 120 paths of the strongest power are extracted for each measurement cycle, namely $L = 120$.

TABLE II
ANGULAR SPREAD

		Tx		Rx	
		$\mu(^\circ)$	$\sigma(^\circ)$	$\mu(^\circ)$	$\sigma(^\circ)$
Measurement	LOS	1.58	0.21	1.77	0.15
	NLOS	1.61	0.23	1.91	0.19
M. 2135	LOS	1.60	0.18	1.62	0.22
	NLOS	1.62	0.25	1.77	0.16

The angular spread are listed in the Table II. As shown in the table, the results estimated are consistent with those from the IMT-Advanced channel model in indoor scenario.

F. Channel Reconstruction

Based on IMT-Advanced channel model, the parameter set extractd from CIRs $\mathbf{H}_{ODA}$ and the measured antenna array radiation patterns $\mathbf{F}^{DPA}$ and $\mathbf{F}^{PIFA}$ are incorporated into the channel model to obtained the reconstructed CIRs. The channel reconstruction follows the form as (1).The antenna pattern $\mathbf{F}_{tx,s}$ at Tx can be rewritten by $\mathbf{F}^{DPA}$, while the antenna patterns $\mathbf{F}_{rx,u}$ at Rx can be rewritten by $\mathbf{F}^{PIFA}$ and $\mathbf{F}^{DPA}$. So the reconstructed CIRs $\mathbf{H}^{model}$ are denoted by $\mathbf{H}_{PIFA}^{model}$ and $\mathbf{H}_{DPA}^{model}$ respectively. Since there are two antenna elements at both sides of the link, $U = S = 2$ in (1).

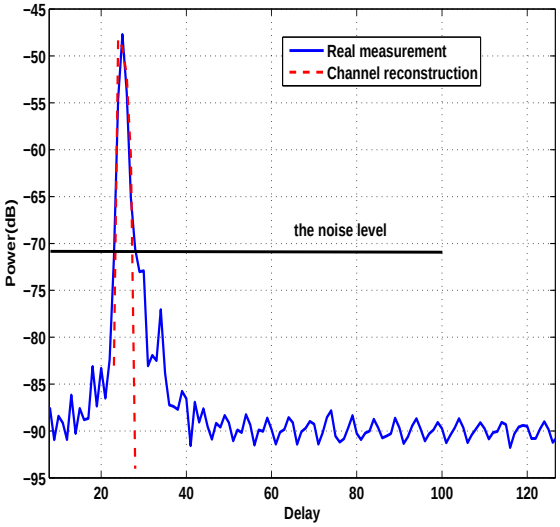

Fig. 3. The delay domain response (in dB) of CIRs

III. ANALYSIS AND RESULTS

A. Coherent Bandwidth

Firstly, the noise level estimation should be done to reduce the affect from the additive noise on inherent characteristic of the channel [14]. For example, the noise level is set to -71dB at spot 4. The reserved power of field CIRs accounts for 96% of the signal with noise. Figures 3 shows the delay domain response of CIRs from the field measurement data $\mathbf{H}_{DPA}^{meas}$ and the reconstructed data $\mathbf{H}_{DPA}^{model}$ with DPAs. It is obvious that above the noise level the reconstructed data can well fit to the field measurement data in delay domain.

Based on the CIRs from the measurement and reconstruction, the power delay profile $\beta(\tau)$ can be calculated as

$$\beta(\tau) = \frac{1}{US} \sum_{u=1}^{U} \sum_{s=1}^{S} |h_{u,s}(\tau)|^2. \tag{2}$$

Then a common normalization of the $\beta(\tau)$ is necessary for the probability density function (pdf) $\overline{\beta}(\tau)$. So the delay spread can be calculated as

$$\sigma_\tau = \sqrt{E(\tau^2) - (E(\tau))^2} \tag{3}$$

where E is expectation operator over all channel realizations. The coherent bandwidth is defined as the bandwidth over which the frequency correlation function is above 0.9, then the coherent bandwidth can be approximately obtained as

$$B_c \approx \frac{1}{50\sigma_\tau}. \tag{4}$$

Since 2×2 antenna configuration is applied in each test case, there are four sub-channels between the transmit-receive antenna pairs in each group of CIRs. Table III shows the coherent bandwidth of each sub-channel (CH1 $\sim$ CH4) for the field CIRs $\mathbf{H}^{meas}$ and the reconstructed CIRs $\mathbf{H}^{model}$. It is shown that the coherent bandwidth of the field measurement CIRs $\mathbf{H}_{DPA}^{meas}$ and the reconstructed $\mathbf{H}_{DPA}^{model}$ are approximated in numerical value. So it is obvious that the reconstruction method based on the IMT-Advanced channel model with DPA will not extend or compress the width of CIRs in delay domain, and will not change the statistical characteristics in frequency domain. But the reconstructed CIRs with PIFA will overestimate the coherent bandwidth, especially in CH2 and CH4. This is because different from the omni-directional antenna gain of dipole antenna the nonideal issues on the PIFA pattern compress the width of CIRs and reduce the dispersion in delay domain. Due to the negligence of nonideal antenna pattern modeling in the IMT-Advanced channel model, the reconstructed data will impose a great impact on the system performance evaluation. In the real environment, the more serious inter-symbol interference (ISI) will cause a degradation in the performance of MIMO-OFDM (Orthogonal Frequency Division Multiplexing) system.

TABLE III
THE COHERENT BANDWIDTH (IN MHZ) IN ALL CASES

		CH1	CH2	CH3	CH4
MEAS	DPA	1.67	1.07	1.24	1.13
	PIFA	1.24	0.83	1.23	0.82
MODEL	DPA	1.26	1.27	1.37	1.28
	PIFA	1.43	1.55	1.34	1.43

B. Eigenvalue Dispersion

To analyze the eigenvalue dispersion and capacity of the channel, the corresponding frequency transfer functions $\mathbf{H}(t, f)$ can be obtained by applying the Fourier transform to the CIRs $\mathbf{H}(t, \tau)$. Assuming that the $\mathbf{H}(j, k)$ is the sample of $\mathbf{H}(t, \tau)$, then

$$\mathbf{H}(j,k) = \mathbf{H}(t,f)|_{t=j\cdot\Delta t, f=k\cdot\Delta f} = \mathbf{H}(j\cdot\Delta t, k\cdot\Delta f) \quad (5)$$

where Δt and Δf are the sampling intervals in time domain and frequency domain, respectively.

For any MIMO transfer matrix at the k^{th} frequency bin of the j^{th} time realization $\mathbf{H}(j, k)$, the singular value decomposition (SVD) can be obtained as

$$\begin{aligned}\mathbf{H}(j,k) &= \mathbf{U}_{SVD}(j,k)\sum(j,k)\mathbf{V}_{SVD}^{H}(j,k) \\ &= \sum_{r=1}^{R}\xi_r(j,k)u_r(j,k)v_r^H(j,k)\end{aligned} \quad (6)$$

where both the $U \times U$ matrix $\mathbf{U}_{SVD}$ and the $S \times S$ matrix $\mathbf{V}_{SVD}$ are unitary matrices, and $\sum(j, k)$ is a $U \times S$ matrix of singular values σ_i of $\mathbf{H}$. These singular values have the property that for ξ_r the r^{th} largest eigenvalue of $\mathbf{HH}^H$. $\xi_1(j,k) \geq \xi_2(j,k) \geq \cdots \geq \xi_R(j,k))$, $1 \leq R \leq \min(U, S)$, are the ordered eigenvalues of the k^{th} frequency bin of j^{th} time channel realization. R is the rank of channel. The eigenvalue dispersion (ED), which is an important metric of MIMO channel, is commonly used to characterize the relative differences between the powers of eigenvalues. In this paper, we use S_{ED} as a metric of ED. The S_{ED} is defined as

$$S_{ED}(j,k) = \frac{\left(\prod_{r=1}^{R}\xi_r(j,k)\right)^{\frac{1}{R}}}{\frac{1}{R}\sum_{r=1}^{R}\xi_r(j,k)} \quad (7)$$

which is the ratio of geometric and arithmetic means of the eigenvalues of $\mathbf{HH}^H$. S_{ED} is a useful figure of merit to characterize ED by a single number [15]. It is noted that in the case of small ED, S_{ED} tends to unity ($S_{ED} \to 1$), whereas, in the case of high ED, S_{ED} tends to zero ($S_{ED} \to 1$).

TABLE IV
THE MEAN VALUE AND STANDARD DEVIATION OF ED

		mean	std
MEAS	DPA	0.65	0.12
	PIFA	0.77	0.12
MODEL	DPA	0.82	0.14
	PIFA	0.82	0.15

Table IV shows the mean value and standard deviation of the eigenvalue dispersion for the field CIRs $\mathbf{H}^{meas}$ and the reconstructed CIRs $\mathbf{H}^{model}$. As is shown in Table IV, for all the four cases, the mean values are respectively 0.65, 0.77, 0.82 and 0.82. This means the reconstructed data have a larger S_{ED} than the real data,so the modeling method underestimates the spatial correlation of MIMO channel. And when take the standard deviation into account, a higher value will cause a significant change in spatial correlation. Compared with the field data, the reconstructed data have a larger standard deviation.

Because of the coupling among the antennas in real environment, the correlation of practical antenna array will increase. However, the IMT-Advanced channel model does not take this nonideal issue into account. This antenna modeling method will make the spatial fading of the parallel channels more independent than real measurement. As the results shown above, using the data from channel reconstruction will underrate the spatial correlation in MIMO system. In order to obtain the expected multiplexing degree from real MIMO system, the more spatial resource (such as antenna spacing and polarized antenna) must be utilized than that used in channel modeling.

$$\sigma_{rms} = \min_{\Delta}\sigma_{rms}(\Delta) = \sqrt{\frac{\sum_{\ell=1}^{L}\left(\varphi_\ell(\Delta) - \mu(\Delta)\right)^2 p_\ell}{\sum_{\ell=1}^{L}p_\ell}}$$

C. Channel Capacity

In the absence of the channel state information at the transmitter, it is optimal to allocate power equally over all antennas.

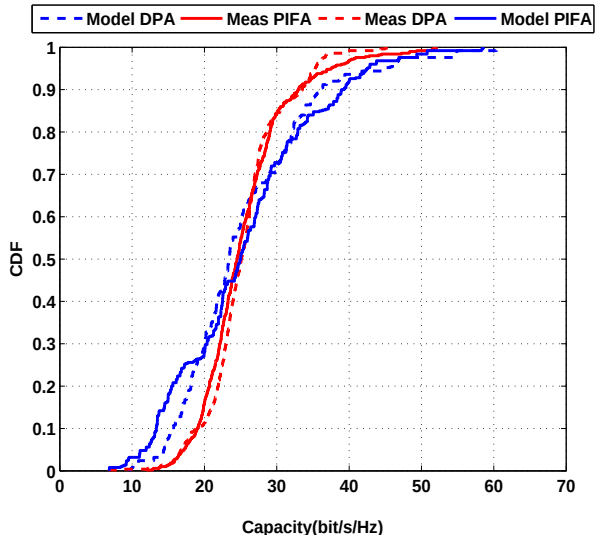

Fig. 4. Capacity CDF at SNR 25 dB

For the discrete channel $H(j,k)$, the channel capacity of frequency-selective fading MIMO channel is given by [16]

$$C(j) \approx \frac{1}{K}\sum_{k=1}^{K}\log_2\det(\mathbf{H}_U + \frac{\rho}{\beta S}\mathbf{H}(j,k)\mathbf{H}^{\mathrm{H}}(j,k)) \quad (8)$$

where ρ denotes the SNR and K is the number of frequency bins of j^{th} time realization and β is a common normalization factor for all channel realizations in such that the average channel power gain is unitary,

$$E\left\{\frac{1}{\beta}\|\mathbf{H}(j,k)\|_F^2\right\} = U \cdot S \quad (9)$$

where $\|\cdot\|_F$ denotes the Frobenius norm. After transforming the transfer matrix to the frequency domain, we can calculate the capacity using (8). Figure 4 shows the capacity cumulative density function (CDF) curves for all cases of channel realizations.Compared the field CIRs with the reconstructed CIRs, it is should be noted that the outage capacity CDF of $\mathbf{H}_{DPA}^{meas}$ has a smaller slope than that of $\mathbf{H}_{DPA}^{model}$. This results in that the field measurement data has a larger 5% channel outage capacity than the reconstructed channel data. The 5% channel outage capacity value of $\mathbf{H}_{DPA}^{meas}$, $\mathbf{H}_{DPA}^{model}$, $\mathbf{H}_{PIFA}^{meas}$ and $\mathbf{H}_{PIFA}^{model}$ are respectively 16.86, 14.62, 17.1 and 12.38. Because the standard deviation of the eigenvalue dispersion from the reconstructed CIRs is larger than that from the field CIRs, the reconstructed data have a larger slope and a higher 5% outage capacity.

IV. Conclusion

In this paper, the antenna pattern modeling of IMT-Advanced channel model is validated by extensive measurement campaign in indoor environment. DPA, PIFA, and ODA are used to collect the spatial CIRs, and the channel reconstruction is performed by updating the characteristics parameters of IMT-Advanced channel model and combined with the antenna array patterns. It is found that the reconstructed data can well fit to the field measurement data in delay domain. But a larger standard deviation of the eigenvalue dispersion makes the reconstructed CIRs have a wider range on spatial correlation than the measured data. On the channel capacity prediction, the wider range on spatial correlation causes the underestimation of the 5% channel outage capacity. So it is concluded that the modeling method based on IMT-Advanced channel model has a larger impact on the spatial characteristics than the frequency characteristics. Because of the nonideal issues on the antennas, the incorporation of the antenna array on the channel model should be further considered for future channel measurement and modeling.

Acknowledgment

The research is supported in part by National Natural Science Foundation of China with NO. 61171105 and by National Key Technology Research and Development Program of the Ministry of Science and Technology of China with NO. 2012BAF14B01, as well as funded by China Academy of Telecommunications Technology.

References

[1] G. Foschini and M. Gans, "On limits of wireless communications in a fading environment when using multiple antennas," *Wireless Personal Communications*, vol. 6, no. 3, pp. 311–335, 1998.

[2] E. Telatar, "Capacity of multi-antenna gaussian channels," *European Transactions on Telecommunications*, vol. 10, no. 6, pp. 585–596, November 1999.

[3] D.-S. Shiu, G. Foschini, M. Gans, and J. Kahn, "Fading correlation and its effect on the capacity of multielement antenna systems," *Communications, IEEE Transactions on*, vol. 48, no. 3, pp. 502 –513, March 2000.

[4] J. Zhang, "Review of wideband mimo channel measurement and modeling for imt-advanced systems," *Chinese Science Bulletin*, vol. 57, pp. 2387–2400, 2012.

[5] D. Chizhik, F. Rashid-Farrokhi, J. Ling, and A. Lozano, "Effect of antenna separation on the capacity of blast in correlated channels," *Communications Letters, IEEE*, vol. 4, no. 11, pp. 337 –339, nov. 2000.

[6] K. Yu, M. Bengtsson, B. Ottersten, D. McNamara, P. Karlsson, and M. Beach, "A wideband statistical model for nlos indoor mimo channels," in *Vehicular Technology Conference, 2002. VTC Spring 2002. IEEE 55th*, vol. 1, 2002, pp. 370 – 374 vol.1.

[7] H. Ozcelik, M. Herdin, W. Weichselberger, J. Wallace, and E. Bonek, "Deficiencies of 'kronecker' mimo radio channel model," *Electronics Letters*, vol. 39, no. 16, pp. 1209 – 1210, aug. 2003.

[8] M. Steinbauer, A. Molisch, and E. Bonek, "The double-directional radio channel," *Antennas and Propagation Magazine, IEEE*, vol. 43, no. 4, pp. 51 –63, aug 2001.

[9] A. M. Shirook M. Ali and P. Lusina, "User effects on mimo performance from an antenna to a link perspective," *International Journal of Antennas and Propagation*, vol. 2011, p. 13, 2011.

[10] *FEKO User Manual, Suite 5.4*, EM Software & Systems-S.A. (Pty) Ltd, 2008.

[11] Y. Zhang, J. Zhang, G. Liu, X. Gao, and P. Zhang, "A generic validation framework for wideband mimo channel models," in *Vehicular Technology Conference, 2008. VTC Spring 2008. IEEE*, may 2008, pp. 330 –334.

[12] *Guidelines for evaluation of radio interface technologies for IMTAdvanced*, ITU-R Std., 2008.

[13] *Propsound cs: The ultimate technology in radio propagation measurement*, Elektrobit.

[14] X. Nie, J. Zhang, C. Huang, Z. Liu, and P. Zhang., "Spatial characteristics and capacity investigation of indoor hotspot channel based on wideband mimo measurement at 4.9 ghz," *Journal of China Universities of Posts and Telecommunications*, vol. 17, pp. 38–44, 2010.

[15] P. Suvikunnas, J. Salo, L. Vuokko, J. Kivinen, K. Sulonen, and P. Vainikainen, "Comparison of mimo antenna configurations: Methods and experimental results," *Vehicular Technology, IEEE Transactions on*, vol. 57, no. 2, pp. 1021 –1031, march 2008.

[16] A. Paulraj, R. Nabar, and D. Gor, *Introduction to Space-Time Wireless Communications*. Cambridge University Press, 2003.